Atmos. Meas. Tech. Discuss., 5, 6991–7023, 2012
www.atmos-meas-tech-discuss.net/5/6991/2012/
doi:10.5194/amtd-5-6991-2012

Atmospheric Measurement Techniques Discussions

Aerosol absorption retrieval at ultraviolet wavelengths in a complex environment

S. Kazadzis[1], N. Kouremeti[2], V. Amiridis[3], A. Arola[4], and E. Gerasopoulos[1]

[1]Institute of Environmental Research and Sustainable Development, National Observatory of Athens, Greece
[2]Laboratory of Atmospheric Physics, Aristotle University of Thessaloniki, Greece
[3]Institute of Astronomy Astrophysics, space applications and remote sensing, National Observatory of Athens, Greece
[4]Finnish Meteorological Institute, Kuopio Unit, Finland

Received: 3 September 2012 – Accepted: 10 September 2012 – Published: 21 September 2012

Correspondence to: S. Kazadzis (kazadzis@noa.gr)

Published by Copernicus Publications on behalf of the European Geosciences Union.

Abstract

We have combined sun and sky radiance measurements from a CIMEL sunphotometer and total and diffuse UV irradiance measurements with a multi-filter rotating shadow-band radiometer (UVMFR), in order to calculate aerosol absorption properties (single scattering albedo) in the UV range, for a 10 month period in Athens, Greece. The aerosol extinction optical thickness measured by the CIMEL instrument has been used for the inter-calibration of the UVMFR. The measurements from both instruments were used as input to a radiative transfer model and the single scattering albedo (SSA) for 368 nm and 332 nm has been calculated. The SSA values at these wavelengths, together with synchronous SSA, CIMEL-derived, retrievals at 440 nm, show a mean of 0.88, 0.86 and 0.80, with lowest values (higher absorption) towards lower wavelengths. In addition, noticeable diurnal variations of the SSA in all wavelengths are revealed, with amplitudes in the order of 0.05. Higher SSA wavelength dependence is found for cases of lower Ångström exponents and also an SSA decrease with decreasing extinction optical depth, suggesting an effect of the different aerosol composition.

1 Introduction

The role of aerosols, both natural and anthropogenic, is extremely important for regional and global climate change studies as well as for overall pollution mitigation strategies. However, a considerable amount of work still needs to be carried out, particularly as it appears that climate change is accelerating with aerosols impacting every, local, regional and global scale. Furthermore, the components controlling aerosol forcing account for the largest uncertainties in relation to anthropogenic climate change (IPCC, 2007). A recent comprehensive review of the assessment of the aerosol direct effect, its state of play as well as outstanding issues, is given by IPCC (2007) and Yu et al. (2006). Both emphasize that the significant aerosol absorption uncertainties in global single scattering albedo (SSA), may constitute the largest single source of

uncertainty in current modeling estimates of aerosol climate forcing. SSA is the ratio of scattering to total extinction (scattering plus absorption). Since both quantities depend strongly on chemical composition, particle size, mixture, relative humidity and wavelength, comprehensive measurements are crucial to understand their effects and to reduce SSA uncertainties that propagate into aerosol radiative forcing estimates.

In the visible (VIS) part of the spectrum, advanced retrieval algorithms for microphysical aerosol properties have been developed in the framework of AERONET (e.g. Dubovik and King, 2000; Nakajima et al., 1996) and all AERONET stations currently provide inversion based VIS-SSA retrievals. More recently, Goering et al. (2005), Taylor et al. (2008) and Kudo et al. (2008) have proposed estimation techniques for the retrieval of spectral aerosol optical properties by combining multi-wavelength measurements using a priori constraints that are applied differently than in the single wavelength methods. The weakness of SSA retrieval is amplified even more in the ultraviolet (UV) part of the spectrum. Compared to the visible spectral region, very little is known about aerosol absorption at UV wavelengths (Krotkov et al., 2005a; Bais et al., 2005; Corr et al., 2009). It is envisaged that improvement in measurement precision and in the general understanding of aerosol absorption in the UV (and immediate derivatives like the SSA) in various scientific applications and based on theoretical assumptions, will contribute significantly to improvement of the accuracy of radiation forcing estimates. For example, desert dust particles (Alfaro et al., 2004), soot produced by fossil fuel burning, and urban transportation, all strongly absorb UV radiation. The optical properties of other potential UV absorbers like organic, nitrate and aromatic aerosols are still poorly known (Bergstrom et al., 2003) though. Recently Bergstrom et al. (2003) showed that spectra of aerosol SSA obtained in different regions of the world varied significantly from region to region, but in ways that could be ascribed to regional aerosol composition. Moreover, recent results from diverse air, ground, and laboratory studies, using both radiometric and in situ techniques, show that the fractions of black carbon, organic matter, and mineral dust in atmospheric aerosols play a role in the determination of the wavelength dependence of aerosol absorption (Russell et al., 2010).

Barnard et al. (2008), exploring the variability of SSA in a case study for the Mexico City metropolitan area, found that, in the near-UV spectral range (250 to 400 nm), SSA is much lower compared to SSA at 500 nm indicative of enhanced absorption in the near-UV range. They suggested that absorption by elemental carbon, dust, or gas alone cannot account for this enhanced absorption leaving the organic carbon component of the aerosol as the most likely absorber.

Ultraviolet (UV) solar radiation has a broad range of effects on life on Earth (UNEP et al., 1998, 2007; UNEP, 2003). It influences not only human beings (e.g. Diffey, 1991), but also plants and animals (e.g. Bornman and Teramura, 1993). Furthermore, it causes degradation of materials and functions as a driver of atmospheric chemistry. There are various studies linking changes of the UV radiation field with changes in the scattering and absorption of aerosols in the atmosphere (e.g. Zerefos et al., 2012). Such changes can be comparable in magnitude with those caused by the decline in stratospheric ozone (Elminir, 2007; Reuder and Schwander, 1999; Krotkov et al., 1998). Moreover, UV variations caused by changes in aerosol optical properties directly affect tropospheric photochemistry:

- increases in regional O_3 (10–20 ppb for Eastern USA) caused by increased UV levels due to the presence of non-absorbing aerosols (Dickerson et al., 1997),
- decreases in regional O_3 (up to 50 ppb for Mexico City and for particular days) caused by strong UV reduction due to absorbing aerosols (Castro et al., 2001).

There are also several more scientific issues that may be clarified with accurate knowledge of aerosol absorption properties:

- aerosol effects on UV trends may enhance, reduce or reverse effects of stratospheric ozone change.

Future scenarios for simulations of global UV levels are based on ozone recovery, having as their sole input the predicted future decline in columnar ozone. Furthermore, simulations of observed tendency of reduced anthropogenic aerosols in the atmosphere

in the US and Europe during the course of the last decade (den Outer et al., 2005) included only cloud and AOD changes in the characterization of likely UV trends. In this regard, changes in the absorbing properties of aerosols on global scales would have had a large effect on the uncertainty budget in any of the above simulations (WMO, 2003). For example, a decrease in aerosol absorption properties accompanied by an AOD decrease in Europe could lead to a significant acceleration of the calculated ozone decline related to UV upward trends (Kazadzis et al., 2009; Zerefos et al., 2012).

– Solar irradiance satellite retrieval algorithms are directly affected by the presence of absorbing aerosols.

The discrepancies between ground-based (GB) UV measurements and satellite-derived (OMI, TOMS, GOME) data are directly related to aerosol absorption that is absent from satellite retrieval algorithms (Tanskanen et al., 2007; Arola et al., 2005). It has been shown that enhanced aerosol UV absorption in urban areas can cause up to 30 % overestimation in the satellite retrieved UV radiation (Kazadzis et al., 2009).

– Uncertainty on commonly used atmospheric radiative transfer applications and codes.

Radiative transfer algorithms calculating UV irradiance, suffer in precision due to large uncertainties in the input parameters (e.g. levels of ozone, aerosol composition and the surface albedo) used in model calculations. It is now known that the major input source of uncertainty in radiative-transfer model simulations, is aerosol absorption (e.g. Van Weele et al., 2000). In particular, the direct radiative effect of aerosols is very sensitive to SSA. For example, a change in SSA from 0.9 to 0.8 can often alter the sign of the direct effect (Yu et al., 2006). Furthermore, the availability and the quality of observational SSA data do not match with hat available for AOD (Krotkov et al., 2005a). This is compounded by the lack of information on the vertical profile of aerosol optical

properties such as the SSA at global scales. Only few case studies have dealt with such measurements and have been limited to local scales (Müller et al., 1999).

The major parameters that describe radiation and aerosol interactions, are the aerosol optical depth (τ), the SSA and the asymmetry parameter (g). The aerosol optical depth at a wavelength λ is the integral of the aerosol extinction coefficient ($b$ext(λ)) over a certain atmospheric layer (in the height range z_1 to z_2).

$$\tau = \int_{z1}^{z2} b_{\text{ext}}(\lambda) \cdot \mathrm{d}z \tag{1}$$

The SSA at a wavelength λ provides the contribution of aerosol particle scattering relative to the total extinction (absorption plus scattering),

$$\text{SSA} = \frac{b_{\text{sca}}(\lambda)}{b_{\text{abs}}(\lambda) + b_{\text{sca}}(\lambda)} \tag{2}$$

Values for the SSA range from 0 (absorbing aerosols only) to 1 (no absorption). The asymmetry parameter, is the phase function (P) weighted average of the cosine of the scattering angle (θ) over all directions. Assuming azimuthal symmetry, the scattering angle integration extends from $-\pi$ to $+\pi$ such that the asymmetry parameter (g) is given by

$$g = 1/2 \cdot \int_{-\pi}^{\pi} \cos\theta \cdot P(\theta) \cdot \sin\theta \cdot \mathrm{d}\theta \tag{3}$$

Values for g range from −1 (backscattered radiation only) to 1 (forward scattered radiation only).

Corr et al. (2009) have presented a review of studies estimating SSA at different wavelengths. For the visible part of the spectrum, two different approaches have been

presented. The first (Dubovik et al., 2002), introduced sky radiance measurements in a matrix inversion technique to calculate various aerosol microphysical properties. This methodology has been widely applied in the Aerosol Robotic Network (AERONET). The second (Kassianov et al., 2005), proposed the use of radiative transfer model (RTM) calculations, using as input measurements of AOD and the ratio of direct to diffuse irradiance at specific wavelengths. However, in the case of SSA calculations at UV wavelengths, enhanced measurement uncertainties, RTM input assumptions, and interference of absorption by other gases (O_3, NO_2), make the retrieval more difficult. All reported results concerning UV-SSA, utilize RTM combined with total and diffuse relative irradiance measurements (Petters et al., 2003; Krotkov et al., 2005b; Corr et al., 2009; Bais et al., 2005) or absolute irradiance measurements (Kazadzis et al., 2010; Ialongo et al., 2010; Bais et al., 2005). The review made by Corr et al. (2009) also presents the major differences in the results of simulations of the SSA, arising from RTM input assumptions, measurement techniques and retrieved wavelengths. Another problem is that previous studies have dealt with short time periods due to the limited lifespan of experimental campaigns.

In this work, for the calculation of the UV-SSA, we adopt a methodology based on the work of Krotkov et al. (2005a,b) and Corr et al. (2009). The methodology, together with the retrieval tools used and technical assumptions made are presented in Sect. 2. The results of UV-SSA measurements their comparison with synchronous AERONET measurements in the visible range are presented in Sect. 3. Finally, discussion of the observed diurnal SSA patterns in Athens, SSA wavelength dependency as well as overall conclusions are presented in the last section of this work.

2 Instrumentation and retrieval methodology

2.1 Instrumentation

In this work we present estimates of SSA at two independently retrieved UV wavelengths 332 nm and 368 nm for an urban site situated in Athens, Greece. The period of measurements analyzed is from January to October, 2010. Since February 2009, the ground-based Atmospheric Remote Sensing Station (ARSS) has been in continuous operation to monitor ground radiation levels and aerosol loadings over Athens (Amiridis et al., 2009). ARSS is located on the roof of the Biomedical Research Foundation of the Academy of Athens (37.9° N, 23.8° E, 130 m a.s.l.) and the campus is located near the city center, 10 km from the sea (Gerasopoulos et al., 2009). ARSS is equipped with a CIMEL CE318-NEDPS9 sun photometer for the retrieval of AOD at 8 wavelengths in the range 340 nm to 1640 nm, including polarization measurements. The technical specifications of the instrument are given in detail by Holben et al. (1998). The CIMEL instrument is part of NASA's AERONET (http://aeronet.gsfc.nasa.gov). ARSS is also equipped with an Ultraviolet Multi-filter Radiometer (UVMFR) instrument for radiation measurements in the UV spectral region (Harrison et al., 1994). UVMFR measures both total and diffuse irradiance at 7 specified wavelengths (300, 305.5, 311.4, 317.6, 325.4, 332.4, and 368 nm) with a 2 nm nominal full width at half maximum (FWHM) bandwidth. Measurements of total and diffuse irradiance are recorded every 10 s, and stored as 1 min averages along with a computation of the direct irradiance. For this work, we have used measurements of the two aforementioned instruments in conjunction with RTM calculations that have been performed using the Libradtran code (Mayer and Kylling, 2005).

2.2 Retrieval methodology

SSA is a key aerosol optical property and describes the portion of solar irradiance that is scattered from the main direct beam passing through the atmosphere. Changes in

SSA influence mostly the diffuse radiation reaching the Earth's surface, while its effect on direct radiation can be considered negligible. SSA values in the atmosphere range from 0.5 to 1.0 at visible wavelengths. The SSA calculated here differs from in situ SSA values retrieved from absorption and scattering measurements at a single altitude level (e.g. at the ground), in that it is a columnar measurement. It therefore represents the "effective" SSA arising from solar irradiance attenuation along a fixed aerosol path.

Model calculations can be used for retrieving SSA when global and/or diffuse spectral irradiance, solar zenith angle (SZA), total column ozone, and AOD are known (Krotkov et al., 2005b; Kazadzis et al., 2010; Ialongo et al., 2010; Corr et al., 2009; Bais et al., 2005). For the retrieval methodology we have used the basic approach that is described in detail in the Corr et al. (2009), Krotkov et al. (2005a,b). This approach consists of measurements of the direct to global ratios (DGR) and AODs measured with the UVMFR instrument that are used as basic input parameters to the RTM for the calculation of the SSA at 332 nm, and 368 nm. Global irradiance measurements from the UVMFR have been used in order to distinguish cloud free conditions for each of the one minute measurements. Clouds are detectable in the measured UVMFR global irradiance (GI) (at 368 nm) since they cause larger variability than aerosols. For distinguishing between cloudy and cloud free conditions, we have applied an updated version of the method of Gröbner et al. (2001). The method is based on the comparison of the measured global irradiance with radiative transfer calculations for cloud free conditions and quality assurance is checked by the following criteria:

(a) the measured GI has to lie within the modeled (cloud free) GI for a range of aerosol loads (AOD at 500 nm of 0.1 and 0.8, respectively), corresponding to the 5th and 95th percentile of the AERONET data for the examined location and period,

(b) the rate of change in the measured GI with SZA has to be within the limits depicted by the modeled cloud free GI, otherwise the measurements are assumed to be contaminated by clouds.

(c) All measured GI values within a time window (dt = ±10 min) should be within 5 % of the modeled cloud free GI, and adjusted to the level of the measurement, using an integral over dt.

If at least 85 % of the points in dt pass tests (a)–(c), then the central point is flagged as cloud free. In this study, we have allowed a tolerance level of ±10 % for tests (a) and (b) in order to compensate for differences between the modeled GI and measured GI due to instrumental uncertainties, as well as for usage of average climatological parameters (constant total ozone column, SSA, etc.) as inputs to the model. We have limited the method to SZA < 80 degrees to avoid uncertainties related with low solar irradiance levels. An example of the results of the method is presented in Fig. 1 for a day with variable cloudiness.

Measurements of the diffuse and global irradiance from the UVMFR have been used in order to retrieve the direct irradiance at 332 nm and 368 nm. Based on the method of Krotkov et al. (2005a), an adjustment in the UVMFR calibration was performed based on synchronous UVMFR and CIMEL measurements. The mean AOD calculated from the 1 min UVMFR measurements within ±5 min from the CIMEL measurement (when the UVMFR 10 min period is characterized by cloudless conditions) has been defined as synchronous. Since the CIMEL instrument provides measurements of AOD at 340 nm and 380 nm, we first calculated the CIMEL derived AOD at 332 nm and 368 nm using the wavelength dependence described by the Ångström Exponent (AE) at these wavelengths. Following this, the Beer-Lambert law for the direct sun (UVMFR) was used to calculate the extraterrestrial Langley calibration constants (ETC) for each UVMFR synchronous measurement. Based on the results presented in Fig. 2a, b, we decided to use a single ETC for the whole period and for each wavelength.

The results of this comparison have a Pearson product moment correlation coefficient equal to 0.97 and 0.98, respectively for 332 nm and 368 nm AODs. Mean absolute differences were zero, with standard deviations of 0.021 and 0.017 for the respective wavelengths, well within the CIMEL AOD retrieval uncertainty of ±0.02. The quality of the data produced can be verified by comparing the AOD's retrieved by the

two instruments as a function of SZA (Fig. 3). The stability of the AOD differences as a function of SZA verifies the quality of the calibration of the UVMFR AOD's and the fact that no SZA-dependent errors are included in this procedure. In the figure, AOD's have been grouped in bins of 5 degree (of SZA). The differences shown in Fig. 3 include ETC determination accuracy, the interpolation of CIMEL AOD at 368 nm using the AE, together with instrumental/measurement errors. Using a single UVMFR ETC for the whole period provides very good agreement between the two instruments. However, this may not be the case for all UVMFR instruments using this approach as ETC may suddenly or gradually change especially for longer measurement time series due to instrumental (filter related) changes.

We calculated look up tables (LUT) with the RTM, of DGR at 368 nm and 332 nm as a function of SZA, AOD, SSA, asymmetry factor (g) and total column ozone. CIMEL/AERONET mean daily ozone values and climatological NO_2 values were deployed for the use of the LUT while for g, we used the mean daily value as retrieved at 440 nm from the CIMEL instrument measurements when available and the mean value of the whole period equal to 0.7 (2σ standard deviation of the g during this period was 0.04) otherwise. Using the UVMFR AOD and DGR measurements we then calculated the matching SSA values for each individual UVMFR DGR measurement.

2.3 Retrieval uncertainties

The CIMEL instrument provides SSA inversion retrievals characterized as Level 1.5 and Level 2.0 data.

Level 2.0 data: Level 2.0 (L2) data are recommended by AERONET as they have less uncertainty but are restricted in measurement to SZA > 50°, AOD at 440 nm > 0.4 and homogeneous sky conditions. These limitations make AERONET SSA L2 worldwide measurements unsuitable for:

(a) climatological studies due to the AOD restriction that limits analyses to areas having large average annual AOD's, or to cases of moderate to high aerosol episodes

in specific areas. As an example, for the urban site of Athens which is one of the most polluted cities in Europe, the number of measurements is limited to just 58 for the whole 10 month dataset available.

(b) diurnal variation studies due to the SZA restriction. For mid and low latitude sites, this limitation leads to a severe lack of information on diurnal SSA patterns as there are few wintertime only measurements and close to zero measurements at local noon time.

Level 1.5 data: AERONET Level 1.5 (L1.5) data is provided by AERONET for all AOD's and SZA. In this work L1.5 data were also used with respect to the AOD, SZA and sky homogeneity conditions (sky error) of each individual measurement. The data has been compared with UVMFR retrieved SSA's taking into account limitations related with the retrieval uncertainties.

For UVMFR data the uncertainty of the UVMFR SSA retrieval is related to:

- direct to global irradiance measurements uncertainties,
- RTM input data accuracy.

Direct to global irradiance measurement uncertainties can result to a range of SSA values rather than a single value, that would succeed a match between the measurement and the RTM DGR outputs. This range broadens at low SZA and low aerosol level cases. The RTM inputs that were used for the SSA LUT construction include also an uncertainty budget (AOD, surface albedo, constant aerosol vertical profile, asymmetry factor). Following the uncertainty analysis of Krotkov et al. (2005b), the total uncertainty of the DGR retrieval was calculated to be ±3 %. The impact of this on the SSA calculation is directly connected with AOD levels and the SZA. In Fig. 4 we have calculated the UVMFR SSA retrieval uncertainty for different AOD's and solar zenith angles. In the same figure, the mean AOD's for Athens measured by the UVMFR, at each solar angle are shown.

3 SSA retrieval results

Using the methodology described in the previous section we calculated the SSA at 332 nm and 368 nm using 1 min data from the UVMFR. For the period under investigation, we also calculated the daily mean SSA's at these two wavelengths in the UV band and also the mean daily SSA's in the visible band derived from data provided by the CIMEL (L1.5 and L2 data) operating in Athens' AERONET station (Fig. 5).

The variability of SSA during this period is quite high, ranging from 0.59 (0.74) to 0.96 (0.96) for 332 nm (440 nm) with mean values of 0.88, 0.86 and 0.80 for 440 nm, 368 nm and 332 nm, respectively. Larger SSA variability was found during the winter period and at low SSA values at all wavelengths but also with larger uncertainty due to the lower AOD values at this time of the year.

When calculating diurnal patterns of the SSA at UV and visible wavelengths for the Athens area, we observed a mean diurnal pattern with a variability of the order of 0.05 and having highest absorption (lowest SSA's) ±2 h around noon (Fig. 6). Similar behavior can also be seen from AERONET retrieved SSA's having higher values observed during the early morning and late evening. However, the SZA limitation of the AERONET retrieval methodology leads to lack of measurement points around noon. To investigate the uncertainty in relation to UVMFR retrievals, the diurnal pattern was calculated for different SSA uncertainty bins according to the analysis of the previous section. In general, the daily pattern is clear for each bin and is mirrored by the AERONET inversion retrievals, however the statistical error bars describing the variability of the SSA's during each hourly bin, are quite large.

In order to investigate the possible dependence of SSA on AOD, Fig. 7 shows the synchronous UVMFR and CIMEL SSA retrievals plotted against AOD at 440 nm. We found that in general, SSA decreases with a decrease in extinction optical thickness. We believe that this behavior reflects seasonal changes from summer to winter months in the average aerosol composition in Athens. Indeed, the annual cycle of SSA is the same as the AOD annual cycle having a maximum in summer and a minimum in winter.

Studies of the SSA annual variability for other cities such as Ispra, Italy and Thessaloniki, Greece (Arola et al., 2005) revealed the same trend, with low SSA values (high absorption) associated with low AOD and reminiscent of mostly wintertime cases. In addition, due to the low AOD the uncertainties associated with the data obtained from both retrieval techniques (AERONET and UVMFR), are quite high. For higher AOD, CIMEL retrievals show an almost constant value of the SSA ∼ 0.92 while lower values have been calculated when moving towards shorter wavelengths. Similar results were reported by Krotkov et al. (2005b) when analyzing measurements derived at Washington, USA.

We performed an analysis of the differences of SSA between the visible and the UV parts of the spectrum based on aerosol characteristics using synchronous CIMEL and UVMFR SSA retrievals and an aerosol classification scheme described in detail in Mielonen et al. (2009). There, a classification of AERONET data was used in order to derive 6 aerosol types based on the SSA measurement at 440 nm and the AE that was derived in the 440–870 nm wavelength range. Mielonen et al. (2009) used a visualization of this characterization and compared their results with the CALIPSO (Omar et al., 2005) aerosol classification scheme obtaining good agreement. The visualization was performed by plotting AE versus SSA for individual sites. In addition, the difference between SSA at 440 nm and 1020 nm (similar to the approach applied by Derimian et al., 2008), was implemented to better distinguish fine absorbing aerosols from coarse ones. The main idea was to fill this SSA versus AE aerosol type related "space" with the differences of SSA_{440}–SSA_{368} (SSADIFF) to investigate a possible link between wavelength dependence and aerosol type. In Fig. 8 using the Mielonen et al. (2009) aerosol typing approach, we plot SSADIFF for different classes (colored scale). In addition, actual points of SSA_{440} measured by the CIMEL instrument, are shown in order to categorize Athens results according to the classification scheme.

The results of Fig. 8 show that the ARSS site in Athens is characterized by a mixture of aerosol types with SSA_{440} values spanning all 6 sub-spaces. More specifically, dust cases (mainly during spring) are able to be identified due to the proximity of Athens

to the Saharan desert (Gerasopoulos et al., 2010). Analyzing the wavelength dependence of the SSA, by defining SSADIFF as the difference SSA_{440}–SSA_{368}, there is evidence that high SSADIFF values tend towards dust absorbing cases. That means that the SSA at UV wavelengths is lower by at least 0.05 compared with SSA_{440} for the majority of the cases with AE < 0.7, while 75 % of all such cases (SSADIFF > 0.05) comply with the condition AE < 1. Russel et al. (2010) reported results obtained from diverse datasets showing SSA wavelength dependency from the IR down to visible wavelengths. In addition, Bergstrom et al. (2007) presented SSA spectra for dust-containing aerosols campaigns (PRIDE and ACE-Asia) including AERONET measurements at sites that are affected by dust such as Cape Verde, Bahrain (Persian Gulf) and the Solar Village (Saudi Arabia). Both studies concluded that the SSA spectra for AERONET locations dominated by desert dust, decrease with decreasing wavelength. In addition, Russel et al. (2010) reported that SSA spectra for AERONET locations dominated by urban-industrial and biomass-burning aerosols, decrease with increasing wavelength in line with the results of Bergstrom et al. (2007). Figure 7 also shows that similar SSA values can be found for 440 nm and 368 nm and for fine aerosol cases (AE > 1.4).

The utility of the AE for aerosol scattering is that its value depends primarily on the size of the particles, ranging from a value of 4 for very small particles (Rayleigh scattering) to 0 for very large particles (such as cloud drops). Thus AE for atmospheric aerosol scattering varies between limits specified by particle size. Various studies (e.g. Bergstrom et al., 2007) have used the Ångström Absorption Exponent (AAE) for studying the aerosol absorption wavelength dependence for different aerosol types and mixing. As the absorption AOD is a relatively smooth decreasing function with wavelength, it can be approximated with a power law wavelength dependence via the AAE which is defined as the negative of the slope of the absorption on a log-log plot. Figure 9 shows the temporal variability of $AAE_{(440-870)}$ and $AAE_{(332-440)}$. Measurements of $AAE_{(440-870)}$ are found to lie between 0.9 and 1.5 (2σ) in accordance with the results of Bergstrom et al., (2007). $AAE_{(332-440)}$ in the UV range is very different from that in the visible, with values ranging from 2 to 5 (2σ). A direct comparison reveals

that for the aerosol composition features of Athens, the AAEs are 2 to 4 times higher in the UV range than in the visible. This is due to a combination of the enhanced absorption (lower SSA's) that has been found in the UV, together with higher AOD's in this band. The data presented in Fig. 9 represent daily means of synchronous measurements of the CIMEL and UVMFR instrument. $AAE_{(440-870)}$ is retrieved from AOD and SSA CIMEL data, while $AAE_{(332-440)}$ is calculated using both UVMFR and CIMEL instrument measurements.

Finally, we have calculated mean SSA values for all CIMEL wavelengths (440 nm, 673 nm, 870 nm and 1020 nm) for the whole period under study, and synchronous (5 min SSA averaged around the CIMEL measurement time) UVMFR SSAs at UV (332 nm and 368 nm). The results are shown in Fig. 10. For the whole dataset of SSA retrievals we have used: (a) all points (CIMEL L1.5 and all UVMFR data), (b) measurements retrieved with AOD > 0.2 (reduced uncertainty), and (c) SSA retrievals only for dust cases ($AE_{340-440} < 0.7$). While for all cases the calculated standard deviation is quite high (≥ 0.05), there is a systematic SSA decrease in the UV range, and mean differences of 0.07 and 0.02 have been found when comparing SSA at the visible range and SSA at 332 nm and 368 nm, respectively. Dust cases in particular show a spectral decrease in SSA with decreasing wavelength from 1022 nm (CIMEL) down to 332 nm (UVMFR).

The spectral dependence of the SSA from the visible to the UV wavelengths is in agreement with findings presented by Corr et al. (2009). With the same approach applied to Mexico City where measurements are also influenced by city emissions and blowing dust, Corr et al. (2009) studied the SSA behavior at UV wavelengths and showed that for AOD > 0.1, SSA varied from 0.78 to 0.80 for 332 nm and 368 nm, respectively with enhanced absorption at UV wavelengths relative to the visible wavelengths attributable to these types of aerosols.

4 Conclusions

The advantages of measuring the aerosol absorption (SSA) in the UV with the UVMFR instrument can be summarized as follows:

- the AOD in the UV wavelength range is higher (for the same aerosol mass) than in the visible spectral range
- the surface albedo is much smaller in the UV than in the visible range
- SSA retrievals with the uncertainty of ±0.03 can be derived for SZA > 40 degrees and with an uncertainty of ±0.04 for all SZA where AOD ≤ 0.2
- the UVMFR instrument can be carefully characterized and corrected for known systematic errors by monitoring instrument performance using daily CIMEL intercomparisons and quality checking
- SSA retrievals are stable and repeatable

We have analyzed a 10 month period of UVMFR and CIMEL measurements at the city of Athens retrieving SSA at visible and UV wavelengths based on the effect of SSA on the DGR and a combined inter-calibration of the two instruments. Since the CIMEL retrieval algorithm is more reliable for high SZA, the combination of the two instruments allows for an increase in measurement frequency and the ability to derive the complete diurnal cycle of aerosol absorption. In addition, the spectral differences of the aerosol absorption properties in the visible and UV wavelength range have been investigated, using synchronous CIMEL and UVMFR retrievals. Results of this work confirmed similar results found for Mexico City, Mexico (Corr et al., 2009), Washington DC, USA (Krotkov et al., 2005b) and Rome, Italy (Ialongo et al., 2010), that presented enhanced absorption of aerosols for UV wavelengths. In this study we used a 10 month measurement period with combined UVMFR and CIMEL data in order to investigate possible effects of aerosol type on observed SSA wavelength differences.

The enhanced aerosol absorption found when comparing UV and visible spectrum results, (particularly dust cases), shows that:

- we expect a small systematic overestimation of modeled solar UV irradiance using SSA from the visible range as an input to RTMs
- we expect a possible decrease in specific days/cases of regional O_3 due to the enhanced aerosol absorption
- satellite post-correction validation results including aerosol absorption effects, have to take into account absorption enhancement in the UV range

The differences that have been found here however, are well within the uncertainty of both retrievals as instrumental effects or absolute calibration uncertainties of sky radiances (∼ 5 % for the CIMEL almucantar measurements) might also play an important role when making such comparisons. The coincidence of AOD measurements using a single inter-calibration factor from both instruments for various SZA over the extended 10 month sample period used here, is a sign that no systematic SZA dependent factors, influence the final SSA results.

Following the work of Krotkov et al. (2005b), we have produced a common dataset of SSA values in the UV and visible wavelengths for Athens. The extended dataset significantly improves comparative statistics and provides additional information on the effect of varying background aerosol conditions and higher aerosol absorption than that provided by Washington, DC.

In conclusion, the combined use of CIMEL sun and sky radiance measurements in the visible combined with UVMFR total and diffuse irradiance measurements in the UV, provide an important advantage for remote measurements of column aerosol absorption over the UV-Visible spectral range.

Acknowledgements. S. Kazadzis would like to acknowledge Marie Curie project ACI-UV, PERG05- GA-2009-247492.

References

Alfaro, S. C., Lafon, S., Rajot, J. L., Formenti, P., Gaudichet, A., and Maillé, M.: Iron oxides and light absorption by pure desert dust: an experimental study, J. Geophys. Res.-Atmos., 109, D08208, doi:10.1029/2003jd004374, 2004.

Amiridis, V., Kafatos, M., Perez, C., Kazadzis, S., Gerasopoulos, E., Mamouri, R. E., Papayannis, A., Kokkalis, P., Giannakaki, E., Basart, S., Daglis, I., and Zerefos, C.: The potential of the synergistic use of passive and active remote sensing measurements for the validation of a regional dust model, Ann. Geophys., 27, 3155–3164, doi:10.5194/angeo-27-3155-2009, 2009.

Arola, A., Kazadzis, S., Krotkov, N., Bais, A., Gröbner, J., and Herman, J. R.: Assessment of TOMS UV bias due to absorbing aerosols, J. Geophys. Res.-Atmos., 110, 1–7, 2005.

Bais, A. F., Kazantzidis, A., Kazadzis, S., Balis, D. S., Zerefos, C. S., and Meleti, C.: Deriving an effective aerosol single scattering albedo from spectral surface UV irradiance measurements, Atmos. Environ., 39, 1093–1102, 2005.

Barnard, J. C., Volkamer, R., and Kassianov, E. I.: Estimation of the mass absorption cross section of the organic carbon component of aerosols in the Mexico City Metropolitan Area, Atmos. Chem. Phys., 8, 6665–6679, doi:10.5194/acp-8-6665-2008, 2008.

Bergstrom, R. W., Pilewskie, P., Schmid, B., and Russell, P. B.: Estimates of the spectral aerosol single scattering albedo and aerosol radiative effects during SAFARI 2000, J. Geophys. Res.-Atmos., 108, 8474, doi:10.1029/2002JD002435, 2003.

Bornman, J. F. and Teramura, A. H.: Effects of ultraviolet-B radiation on terrestrial plants, in: Environmental UV-Photobiology, edited by: Young, A. R., Björn, L. O., Moan, J., and Nultsch, W., Plenum Press, New York, 427–471, 1993.

Castro, T., Madronich, S., Rivale, S., Muhlia, A., and Mar, B.: The influence of aerosols on photochemical smog in Mexico City, Atmos. Environ., 35, 1765–1772, 2001.

Corr, C. A., Krotkov, N., Madronich, S., Slusser, J. R., Holben, B., Gao, W., Flynn, J., Lefer, B., and Kreidenweis, S. M.: Retrieval of aerosol single scattering albedo at ultraviolet wavelengths at the T1 site during MILAGRO, Atmos. Chem. Phys., 9, 5813–5827, doi:10.5194/acp-9-5813-2009, 2009.

den Outer, P. N., Slaper, H., and Tax, R. B.: UV radiation in the Netherlands: assessing long-term variability and trends in relation to ozone and clouds, J. Geophys. Res., 110, D02203, doi:10.1029/2004jd004824, 2005.

Derimian, Y., Leon, J. F., Dubovik, O., Chiapello, I., Tanre, D., Sinyuk, A., Auriol, F., Podvin, T., Brogniez, G., and Holben, B. N.: Radiative properties of aerosol mixture observed during the dry season 2006 over M'Bour, Senegal (African Monsoon Multidisciplinary Analysis campaign), J. Geophys. Res., 113, D00C09, doi:10.1029/2008JD009904, 2008.

Dickerson, R. R., Kondragunta, S., Stenchikov, G., Civerolo, K. L., Doddridge, B. G., and Holben, B. N.: The impact of aerosols on solar ultraviolet radiation and photochemical smog, Science, 278, 827–830, 1997.

Diffey, B. L.: Solar ultraviolet-radiation effects on biological-systems, Phys. Med. Biol., 36, 299–328, 1991.

Dubovik, O. and King, M. D.: A flexible inversion algorithm for retrieval of aerosol optical properties from Sun and sky radiance measurements, J. Geophys. Res.-Atmos., 105, 20673–20696, 2000.

Dubovik, O., Holben, B. N., Lapyonok, T., Sinyuk, A., Mishchenko, M. I., Yang, P., and Slutsker, I.: Non-spherical aerosol retrieval method employing light scattering by spheroids, Geophys. Res. Lett., 29, 1415, doi:10.1029/2001GL014506, 2002.

Elminir, H. K.: Sensitivity of ultraviolet solar radiation to anthropogenic air pollutants and weather conditions, Atmos. Res., 84, 250–264, 2007.

Gerasopoulos, E., Kokkalis, P., Amiridis, V., Liakakou, E., Perez, C., Haustein, K., Eleftheratos, K., Andreae, M. O., Andreae, T. W., and Zerefos, C. S.: Dust specific extinction cross-sections over the Eastern Mediterranean using the BSC-DREAM model and sun photometer data: the case of urban environments, Ann. Geophys., 27, 2903–2912, doi:10.5194/angeo-27-2903-2009, 2009.

Goering, C. D., L'Ecuyer, T. S., Stephens, G. L., Slusser, J. R., Scott, G., Davis, J., Barnard, J. C., and Madronich, S.: Simultaneous retrievals of column ozone and aerosol optical properties from direct and diffuse solar irradiance measurements, J. Geophys. Res., 110, D05204, doi:10.1029/2004jd005330, 2005.

Gröbner, J., Kouremeti, N., and Rembges, D.: A systematic comparison of solar UV radiation spectra with radiative transfer calculations, 8th European Symposium on Physico-Chemical Behaviour of Air Pollutants, A Changing Atmosphere EC, ORA/POST 62172, 2001.

Holben, B. N., Eck, T. F., Slutsker, I., Tanré, D., Buis, J. P., Setzer, A., Vermote, E., Reagan, J. A., Kaufman, Y. J., Nakajima, T., Lavenu, F., Jankowiak, I., and Smirnov, A.: AERONET – a federated instrument network and data archive for aerosol characterization, Remote Sens. Environ., 66, 1–16, 1998.

Ialongo, I., Buchard, V., Brogniez, C., Casale, G. R., and Siani, A. M.: Aerosol Single Scattering Albedo retrieval in the UV range: an application to OMI satellite validation, Atmos. Chem. Phys., 10, 331–340, doi:10.5194/acp-10-331-2010, 2010.

Kassianov, E. I., Barnard, J. C., and Ackerman, T. P.: Retrieval of aerosol microphysical properties using surface MultiFilter Rotating Shadowband Radiometer (MFRSR) data: modeling and observations, J. Geophys. Res.-Atmos., 110, 1–12, doi:10.1029/2004jd005337, 2005.

Kazadzis, S., Bais, A., Balis, D., Kouremeti, N., Zempila, M., Arola, A., Giannakaki, E., Amiridis, V., and Kazantzidis, A.: Spatial and temporal UV irradiance and aerosol variability within the area of an OMI satellite pixel, Atmos. Chem. Phys., 9, 4593–4601, doi:10.5194/acp-9-4593-2009, 2009.

Kazadzis, S., Gröbner, J., Arola, A., and Amiridis, V.: The effect of the global UV irradiance measurement accuracy on the single scattering albedo retrieval, Atmos. Meas. Tech., 3, 1029–1037, doi:10.5194/amt-3-1029-2010, 2010.

Krotkov, N., Bhartia, P. K., Herman, J., Slusser, J., Labow, G., Scott, G., Janson, G., Eck, T. F., and Holben, B.: Aerosol ultraviolet absorption experiment (2002 to 2004), part 1: Ultraviolet multifilter rotating shadowband radiometer calibration and intercomparison with CIMEL sunphotometers, Opt. Eng., 44, 1–17, 2005a.

Krotkov, N. A., Bhartia, P. K., Herman, J., Slusser, J., Scott, G., Labow, G., Vasilkov, A. P., Eck, T. F., Dubovik, O., and Holben, B. N.: Aerosol ultraviolet absorption experiment (2002 to 2004), part 2: Absorption optical thickness, refractive index, and single scattering albedo, Opt. Eng., 44, 1–17, 2005b.

Krotkov, N. A., Bhartia, P. K., Herman, J. R., Fioletov, V., and Kerr, J.: Satellite estimation of spectral surface UV irradiance in the presence of tropospheric aerosols, 1. Cloud-free case, J. Geophys. Res.-Atmos., 103, 8779–8793, 1998.

Kudo, R., Uchiyama, A., Yamazaki, A., Kobayashi, E., and Nishizawa, T.: Retrieval of aerosol single-scattering properties from diffuse and direct irradiances: numerical studies, J. Geophys. Res., 113, D09204, doi:10.1029/2007jd009239, 2008.

Mayer, B. and Kylling, A.: Technical note: The libRadtran software package for radiative transfer calculations – description and examples of use, Atmos. Chem. Phys., 5, 1855–1877, doi:10.5194/acp-5-1855-2005, 2005.

Mielonen, T., Arola, A., Komppula, M., Kukkonen, J., Koskinen, J., de Leeuw, G., and Lehtinen, K. E. J.: Comparison of CALIOP level 2 aerosol subtypes to aerosol types derived from

AERONET inversion data, Geophys. Res. Lett., 36, L18804, doi:10.1029/2009gl039609, 2009.

Müller, D., Wandinger, U., and Ansmann, A.: Microphysical particle parameters from extinction and backscatter lidar data by inversion with regularization: simulation, Appl. Optics, 38, 2358–2368, 1999.

Omar, A. H., Won, J. G., Winker, D. M., Yoon, S. C., Dubovik, O., and McCormick, M. P.: Development of global aerosol models using cluster analysis of Aerosol Robotic Network (AERONET) measurements, J. Geophys. Res.-Atmos., 110, D10S14, doi:10.1029/2004JD0048, 2005.

Petters, J. L., Saxena, V. K., Slusser, J. R., Wenny, B. N., and Madronich, S.: Aerosol single scattering albedo retrieved from measurements of surface UV irradiance and a radiative transfer model, J. Geophys. Res. 108, 4288, doi:10.1029/2002JD002360, 2003.

Reuder, J. and Schwander, H.: Aerosol effects on UV radiation in nonurban regions, J. Geophys. Res.-Atmos., 104, 4065–4077, 1999.

Russell, P. B., Bergstrom, R. W., Shinozuka, Y., Clarke, A. D., DeCarlo, P. F., Jimenez, J. L., Livingston, J. M., Redemann, J., Dubovik, O., and Strawa, A.: Absorption Angstrom Exponent in AERONET and related data as an indicator of aerosol composition, Atmos. Chem. Phys., 10, 1155–1169, doi:10.5194/acp-10-1155-2010, 2010.

Tanskanen, A., Lindfors, A., Määttä, A., Krotkov, N., Herman, J., Kaurola, J., Koskela, T., Lakkala, K., Fioletov, V., Bernhard, G., McKenzie, R., Kondo, Y., O'Neill, M., Slaper, H., den Outer, P., Bais, A. F., and Tamminen, J.: Validation of daily erythemal doses from ozone monitoring instrument with ground-based UV measurement data, Validation of daily erythemal doses from ozone monitoring instrument with ground-based UV measurement data, J. Geophys. Res., 112, D24S44, doi:10.1029/2007JD008830, 2007

Taylor, T. E., L'Ecuyer, T. S., Slusser, J. R., Stephens, G. L., and Goering, C. D.: An operational retrieval algorithm for determining aerosol optical properties in the ultraviolet, J. Geophys. Res., 113, D03201, 10.1029/2007jd008661, 2008.

UNEP, van der Leun, J.C., Tevini, M., Tang, X. and Worrest, R.C. (eds.), United Nations Environment Programme, Nairobi, United Nations Environment Programme, 205 pp., ISBN 92-807-1724-3, 1998.

UNEP: Environmental effects of ozone depletion and its interactions with climate change: 2002 assessment, executive summary, Photochem. Photobio. S., 2, 1–4, 2003.

UNEP, Van Der Leun, J., Bornman, J. F., and Tang, X.: Environmental effects of ozone depletion and its interactions with climate change: 2006 assessment, Photochem. Photobiol. Sci., 6, 209–209, doi:10.1039/B700016B, 2007.

Van Weele, M., Martin, T. J., Blumthaler, M., Brogniez, C., Den Outer, P. N., Engelsen, O., Lenoble, J., Mayer, B., Pfister, G., Ruggaber, A., Walravens, B., Weihs, P., Gardiner, B. G., Gillotay, D., Haferl, D., Kylling, A., Seckmeyer, G., and Wauben, W. M. F.: From model intercomparison toward benchmark UV spectra for six real atmospheric cases, J. Geophys. Res.-Atmos., 105, 4915–4925, 2000.

WMO: Scientific Assessment of Ozone Depletion: 2002, Global Ozone Research and Monitoring Project – Report No. 47, Geneva, Switzerland, 498 pp., 2003.

Yu, H., Kaufman, Y. J., Chin, M., Feingold, G., Remer, L. A., Anderson, T. L., Balkanski, Y., Bellouin, N., Boucher, O., Christopher, S., DeCola, P., Kahn, R., Koch, D., Loeb, N., Reddy, M. S., Schulz, M., Takemura, T., and Zhou, M.: A review of measurement-based assessments of the aerosol direct radiative effect and forcing, Atmos. Chem. Phys., 6, 613–666, doi:10.5194/acp-6-613-2006, 2006.

Zerefos, C. S., Tourpali, K., Eleftheratos, K., Kazadzis, S., Meleti, C., Feister, U., Koskela, T., and Heikkilä, A.: Evidence of a possible turning point in solar UV-B over Canada, Europe and Japan, Atmos. Chem. Phys., 12, 2469–2477, doi:10.5194/acp-12-2469-2012, 2012.

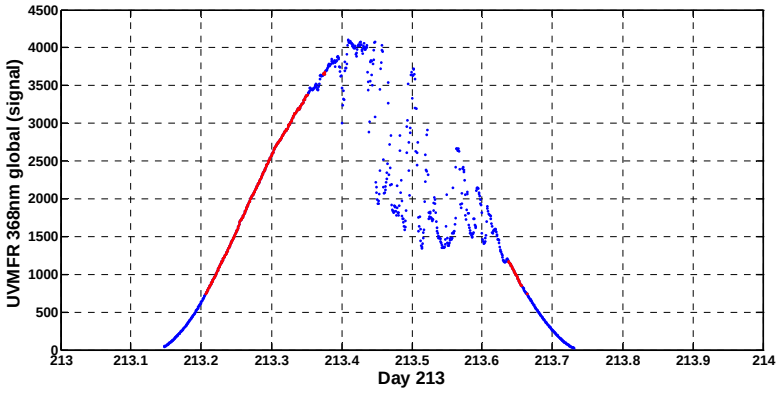

Fig. 1. Determination of cloudless 1-min measurements (red), from all measurements (blue) for a day with variable cloudiness.

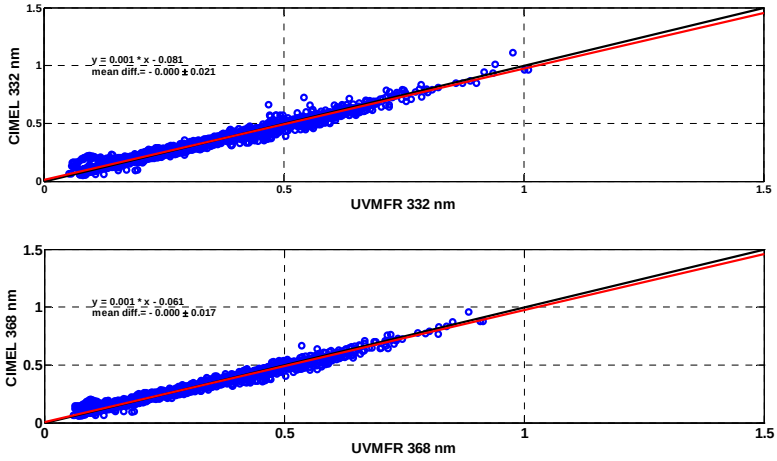

Fig. 2. Comparison of CIMEL and UVMFR retrieved AODs for synchronous measurements for 332 nm (up) and 368 nm (down).

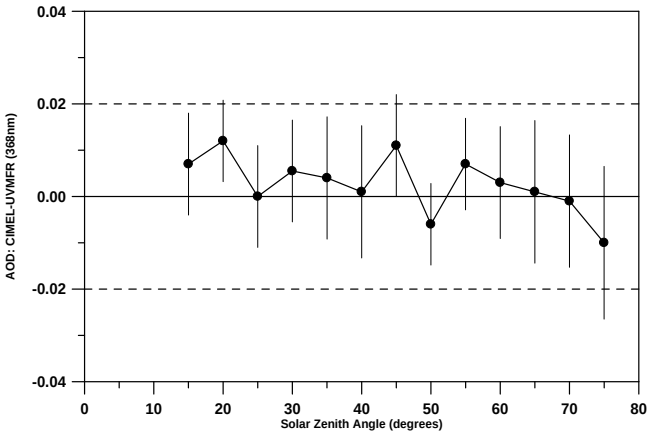

Fig. 3. AOD differences between CIMEL and UVMFR at 368 nm, as a function of solar zenith angle.

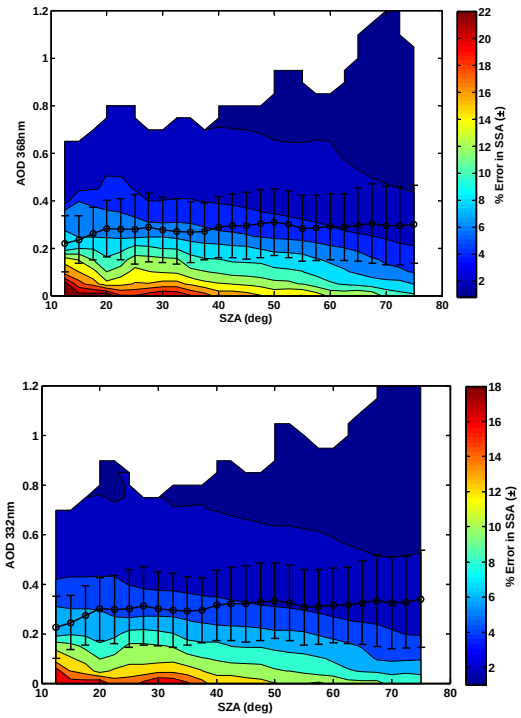

Fig. 4. Error budget (color) for the SSA retrieval from UVMFR as a function of AOD and solar zenith angle for 368 nm (upper panel) and 332 nm (lower panel). Superimposed, mean AODs for 2.5° bins of solar zenith angle are shown.

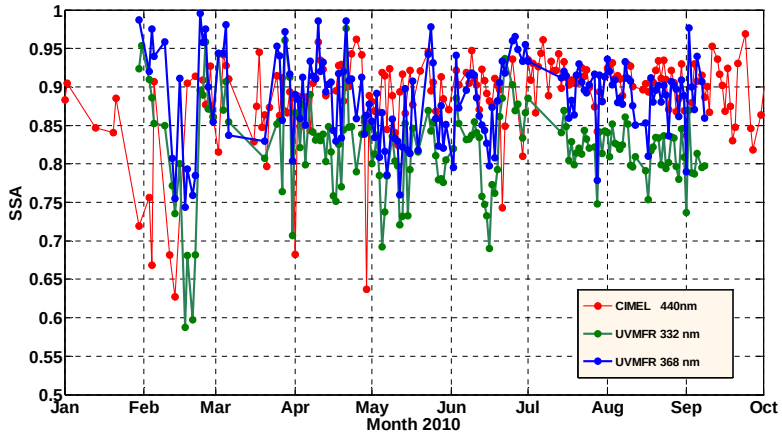

Fig. 5. Mean daily SSAs in the UV (UVMFR) at two wavelengths and the visible range (CIMEL) for Athens area.

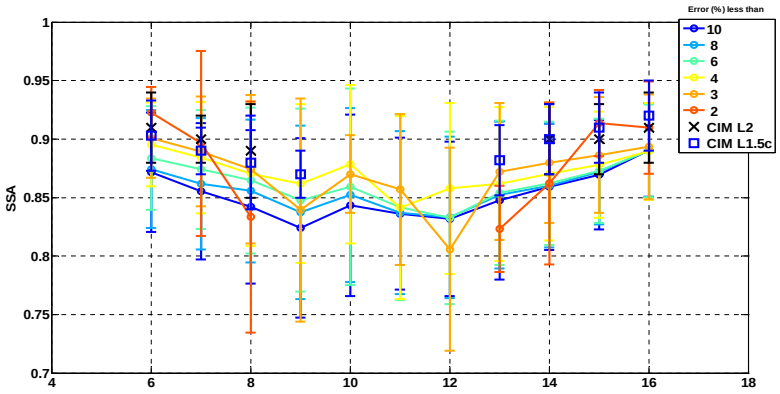

Fig. 6. Diurnal patterns of SSA derived from the UVMFR and CIMEL measurements.

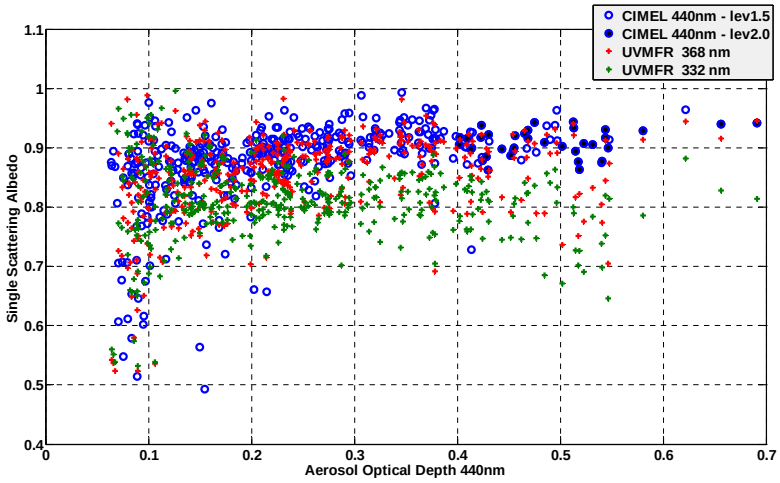

Fig. 7. Dependence of the calculated SSA from AOD measurements.

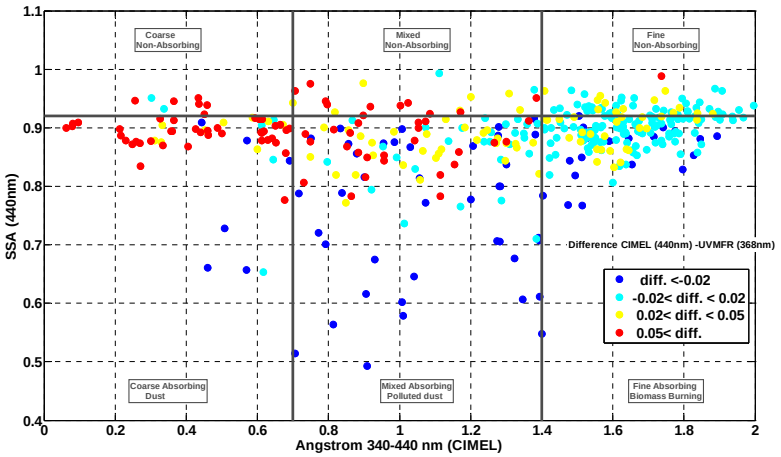

Fig. 8. SSA at 440 nm from the CIMEL instrument as a function of $AE_{(340-440\,nm)}$. Colors represent different ranges of the spectral differences of $SSA_{440\,nm}$–$SSA_{368\,nm}$.

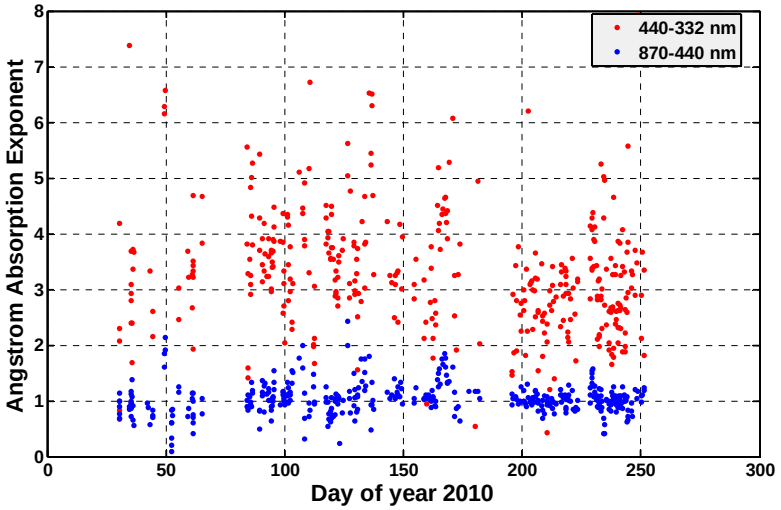

Fig. 9. Daily mean Ångström Absorption Exponent $AAE_{(440-870)}$ and $AAE_{(332-440)}$.

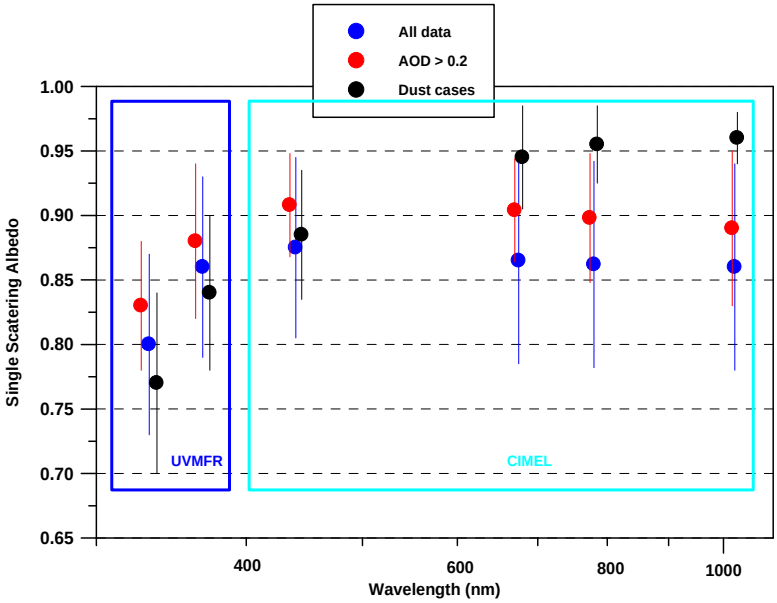

Fig. 10. Wavelength dependence of SSA from synchronous CIMEL and UVMFR measurements. Blue points represent all data points, red data retrievals with AOD > 0.2 and black data only dust aerosol cases.